Mesoporous Materials

DOI: 10.1002/ange.201004972

Single-Crystal-like Titania Mesocages**

Zhenfeng Bian, Jian Zhu, Jing Wen, Fenglei Cao, Yuning Huo, Xufang Qian, Yong Cao, Meiqing Shen, Hexing Li,* and Yunfeng Lu**

Titania represents the most widely used oxide semiconductor for photocatalysts and photovoltaics,[1–12] and its performance is heavily governed by its surface area and the exposed crystal planes.[13–18] To date, however, as-made TiO_2 samples have been limited to the single crystals with low surface area or porous polycrystals exposing their less-active planes. We report herein the synthesis of high-surface-area, single-crystal-like anatase with controlled mesoporous network and preferential exposure of the highly active (001) planes. This simple solution-growth method is readily extendable to the synthesis of other mesoporous single crystals beyond TiO_2, providing a new class of materials for catalysis, energy storage and conversion, and other applications.

The photocatalytic activity of TiO_2 is generally dependent on its crystallography.[13–19] For example, the (001) planes of anatase are much more active than the (101) planes, which are the most commonly observed and thermodynamically more stable crystalline planes in the anatase form.[19] Significant effort has therefore been devoted to synthesize TiO_2 crystals with preferential (001) plane exposure.[5,13–18] As well as crystallographic control, equally important is building networks of pores within the crystals to increase the surface area and provide pore-dependent activity and selectivity.[20–22] To date, although a large number of porous TiO_2 have been made using sol–gel and soft- or hard-templating approaches,[1,6,8,21,23–25] the current materials are limited to porous TiO_2 with amorphous or polycrystalline frameworks that exhibit low photocatalytic activity and charge-transport capability. Herein, using a method of crystal oriented growth, we report the synthesis of highly active mesoporous, single-crystal-like TiO_2 (mesocages) with both preferential (001) plane exposure and controllable mesoporous networks.

As illustrated in Figure 1, we started with precursor solutions containing SO_4^{2-}; solvothermal reactions generate TiO_2 building crystals of which the (001) planes are preferably adsorbed by the SO_4^{2-} anions. Attached growth of the building crystals created crystal clusters with the protected (001) planes (step 1). Further growth led to TiO_2 crystals with preferential (001) plane exposure and disordered mesoporous networks that originate from the voids among the building crystals (step 2). To construct an ordered mesoporous channels, the growth was confined within a scaffold with ordered pore channels, such as the silica containing 2D (SBA-15, *P6mm* space group) and 3D (KIT-6, *Ia3d* space group) ordered mesopores. Subsequent scaffold removal resulted in TiO_2 crystals with replicated 2D hexagonal structure (step 3) or 3D (step 4) ordered network structure, respectively.

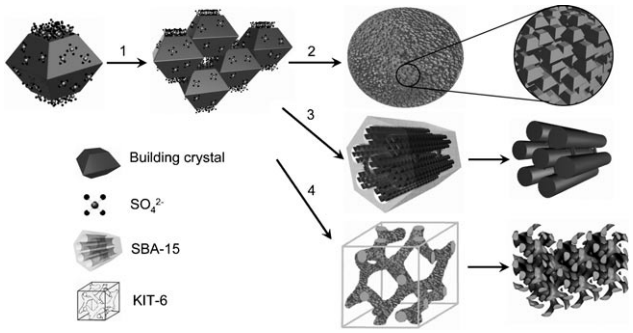

Figure 1. Synthesis of mesoporous single-crystal-like TiO_2. 1) Formation TiO_2 crystal clusters with preferential exposure of the (001) planes from component crystals of which (001) planes were preferably adsorbed with SO_4^{2-}. 2) Further attached growth of crystals leading to the formation of single crystals with preferential (001) planes and disordered mesoporous structure. Crystals with ordered mesoporous structure were prepared by a confined growth of the crystals within 3) SBA-15 (mesoporous silica with 2D pore channels) and 4) KIT-6 (mesoporous silica with ordered 3D pore channels) followed by scaffold removal.

The TiO_2 crystals with disordered mesoporous structure show an average diameter of 600 nm (Figure 2a), and are composed of component crystals with an average diameter of 8.0 nm (Figure 2b). The disordered mesoporous structure is clearly shown by the TEM image (Figure 2c); nevertheless, a selected-area electron diffraction (SAED) pattern recorded on the crystal (inset) shows a diffraction pattern of single-

[*] Dr. Z. Bian, J. Zhu, F. Cao, Y. Huo, X. Qian, Prof. H. Li
The Key Lab of the Chinese Ministry of Education
in Resource Chemistry, Shanghai Normal University
Shanghai 200234 (China)
E-mail: hexing-li@shnu.edu.cn
Prof. Y. Lu
Department of Chemical and Biomolecular Engineering
The University of California, Los Angeles, CA 90095 (USA)
E-mail: luucla@ucla.edu
J. Wen, Prof. M. Shen
School of Chemical Engineering, Tianjin University
Tianjin 300072 (China)
E-mail: mqshen@tju.edu.cn
Prof. Y. Cao
Department of Chemistry, Fudan University
Shanghai 200433 (China)

[**] This work was supported by the National Natural Science Foundation of China (20825724, 20907032) and the Shanghai Government (0952nm00500, 09520715300, 07dz22303, and S30406).

Supporting information for this article is available on the WWW under http://dx.doi.org/10.1002/anie.201004972.

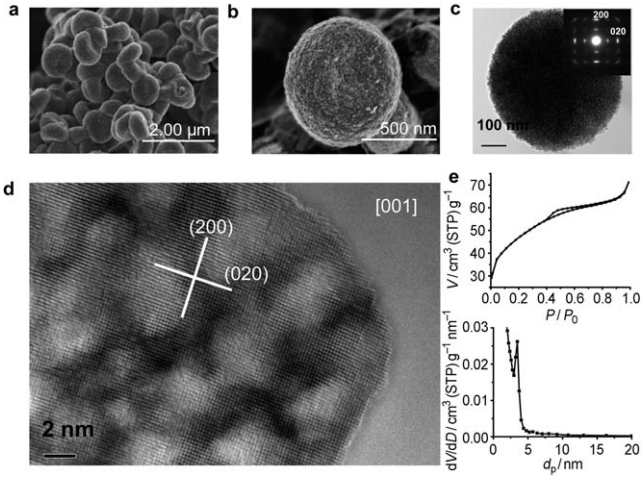

Figure 2. Single-crystal-like TiO_2 with disordered mesopores. a) Scanning electron microscopy (SEM) image of the crystals showing an ellipsoid morphology. b) Magnified SEM image of a crystal clearly revealing its formation from small component nanocrystals. c) Transmission electron microscopy (TEM) image of a representative crystal showing a disordered mesoporous structure and the selected area electron diffraction (SAED) pattern (inset) showing a single-crystal diffraction along the anatase [001] zone axis. d) High-resolution TEM (HRTEM) image of the edge of a TiO_2 crystal showing highly ordered lattices recorded from [001] orientation and embedded mesoporous networks. e) N_2 adsorption–desorption isotherms and pore size distribution of the single crystals at 77 K. V = volume; P/P_0 = relative pressure; d_p = pore diameter.

crystal anatase along the [001] zone axis. HRTEM image (Figure 2d) further shows the single-crystal lattices with embedded 3–4 nm mesopores; the measured lattice spacing of 1.89 Å and angle of 90° is consistent with the anatase (200) and (020) planes.[5,18] Combining the crystal morphology with SAED patterns from the [001] and [101] zone axis (Figure S1 in the Supporting Information) suggests the formation of single-crystal TiO_2 with (001) facet exposure. Consistently, these crystals show a type-IV isotherm (Figure 2e) with a high surface area of 180 $m^2 g^{-1}$ and uniform pore diameter of 3.4 nm. Note that the pore volume and surface area of the crystals would be altered by using different solvents (Table S2). X-ray diffraction (XRD) analysis shows intense reflections of anatase and one reflection at low two-theta value (ca. 0.85°), thus confirming the mesoporous structure (Figure S2). As shown in Figure 2a, the crystals exhibit a unique spheroid shape, which may be attributed from their formation pathway, namely, oriented growth of the building crystals into self-similar crystals.[26] Although stacking of the building crystals into single crystals may prefer a cube shape consistent with their crystallographic structure, it is also thermodynamically favorable to minimize the surface energy by adapting a spherical shape. It is therefore believed that balancing both effects led to the formation of such unique spheroid shape. Nevertheless, to distinguish such crystals from the traditional single crystals, we termed these crystals "single-crystal-like" crystals.

Confined growth within SBA-15 leads to single-crystal-like TiO_2 with replicated 2D mesostructure. These crystals are composited with TiO_2 nanorods hexagonally arranged along the [110] (Figure 3a) and [001] (Figure 3b) zone axes of SBA-15, respectively, which was further confirmed by SAED (bottom inset in Figure 3a and the inset in Figure 3b). The

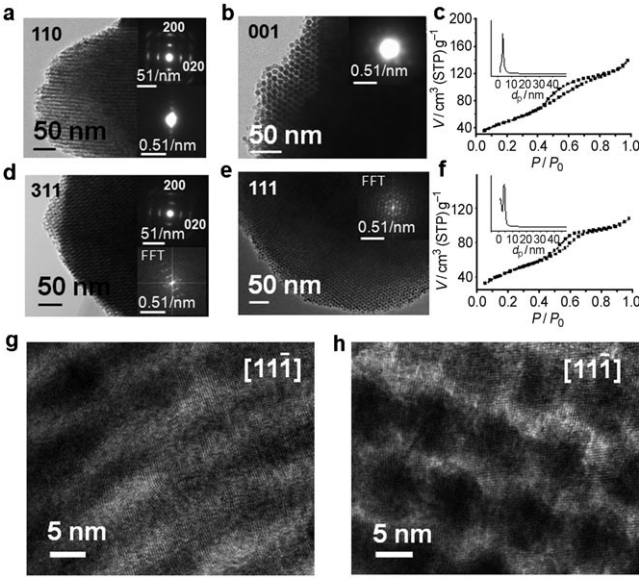

Figure 3. Single-crystal-like TiO_2 with ordered mesopores. TEM images and nitrogen sorption isotherms of mesoporous single crystals grown within the SBA-15 (a, b, c, g) and KIT-6 (d, e, f, h) followed by removal of the scaffold. The pore size distributions are shown as the inset in (c) and (f), respectively. The insets shows (top a, top d) single-crystal SAED patterns along the anatase [001] zone axis confirming the formation of single-crystal anatase, and (b, bottom a) SAED patterns of the hexagonal mesostructure of the crystals along the (110) and (001) axes of the mesophase. The insets (e, bottom d) show fast Fourier transform (FFT) diffractograms confirming the formation of ordered 3D mesoporous structure. The TEM images were taken along a) [110], b) [001], d) [311], and e) [111] zone axes of the mesostructure. The formation of single-crystal-like TiO_2 was further confirmed by the high-resolution TEM (HRTEM) images (g, h) showing highly ordered anatase [11$\bar{1}$] planes.

diameter of these nanorods is 6.1 nm, which is consistent with the pore diameter of SBA-15 (6.3 nm). The SAED pattern (top inset, Figure 3a) of the crystal exhibits a similar single-crystal pattern; nitrogen sorption show uniform pore diameter around 4.6 nm and a surface area of 179 $m^2 g^{-1}$, which is consistent with the pore-wall thickness of SBA-15 (4.7 nm; Figure 3c, Table S1). Similarly, confined growth with KIT-6 led to TiO_2 crystals with ordered 3D mesoporous cages. Highly ordered mesostructure is observed along the [311] and [111] zone axes of KIT-6 (Figure 3d,e), and the single-crystal structure is confirmed by SAED analysis (top inset, Figure 3d). A nitrogen sorption experiment exhibits a typical mesoporous isotherm with uniform pore diameter around 4.6 nm and a high surface area of 165 $m^2 g^{-1}$, which are consistent with the mesoporous structure of the scaffold (Figure 3f, Table S1). The formation of TiO_2 crystals with ordered mesocages was further confirmed by HRTEM (Figure 3g,h), exhibiting ordered mesoporous channels within the continuous single-crystal lattices. Consistently,

XRD shows the reflections of anatase (Figure S3) and the mesostructure consistent with the SBA-15 (100) (Figure S4a) and the KIT-6 (211) reflection (Figure S4b), respectively.[27,28]

To understand the formation mechanism, we compared the TEM images and SAED patterns (insets) of the crystals for different synthesis times (Figure 4a). The growth started with an amorphous structure after 1 hour of reaction. A crystalline structure was observed after 24 h, and perfected to a single-crystal structure after 48 h, and remained unchanged after 336 h. Therefore, step growth from amorphous clusters to nanocrystals to single crystals is proposed. Firstly, clusters of TiO_2 were formed through hydrolysis and condensation of the precursor. Then, the clusters within the amorphous particles further crystallized to form nanocrystals, as confirmed by TEM and SEM observations (Figure 2b,c). For further verification, Figure 4b shows a TEM image of dispersed crystals with uniform 5 nm sizes synthesized at lower precursor concentration. The adjacent nanocrystals attach with each other along their (101) planes into single crystals while leaving their protected (001) planes exposed. Indeed, as shown in the Figure S2, the XRD reflection at $2\theta = 0.85°$ confirms the ordered arrangement of the component crystals. These component crystals were then fused into a continuous single-crystalline structure (Figure 2d). In fact, truncated octahedral TiO_2 component crystals were observed by HRTEM; it was therefore believed that oriented stacking of these component crystals leads to the single-crystal-like structure with preferable exposure of {001} facets (see Figure S5). This synthetic scheme can be extended to synthesize of a family of mesoporous oxide single crystals, such as ZrO_2 and CeO_2 (Figure 4c,d, and Figure S6), ZnO, and In_2O_3.

It was found that single crystals form only in the presence of SO_4^{2-} or F^-. Using $TiCl_4$ or any titanium alkoxide as precursor led only to polycrystalline structures (Figure S7a,b); adding SO_4^{2-} or F^- resulted in single crystals (Figure S7c–f). To understand this phenomenon, ζ potentials of polycrystalline TiO_2 in the presence of AcOH, H_3PO_4, HCl, HNO_3, H_2SO_4, or HF were measured (Figure 4e). Note that anatase has an isoelectric point of 4.0 (positive ζ potential at $pH \approx 1$). Dramatically lower ζ potentials were observed in the presence of H_2SO_4 (−28 mV) and HF (−33 mV), relative to the others (−5 to 10 mV), indicating the significant adsorption of SO_4^{2-} and F^-. It has been well documented that titania (001) planes are generally more active for anion adsorption than other planes; the higher density of fivefold Ti on the (001) surfaces leads to greater adsorption of SO_4^{2-} and F^-.[18] The effective SO_4^{2-} and F^- adsorption on the (001) planes protects the (001) planes, enabling their preferential exposure.

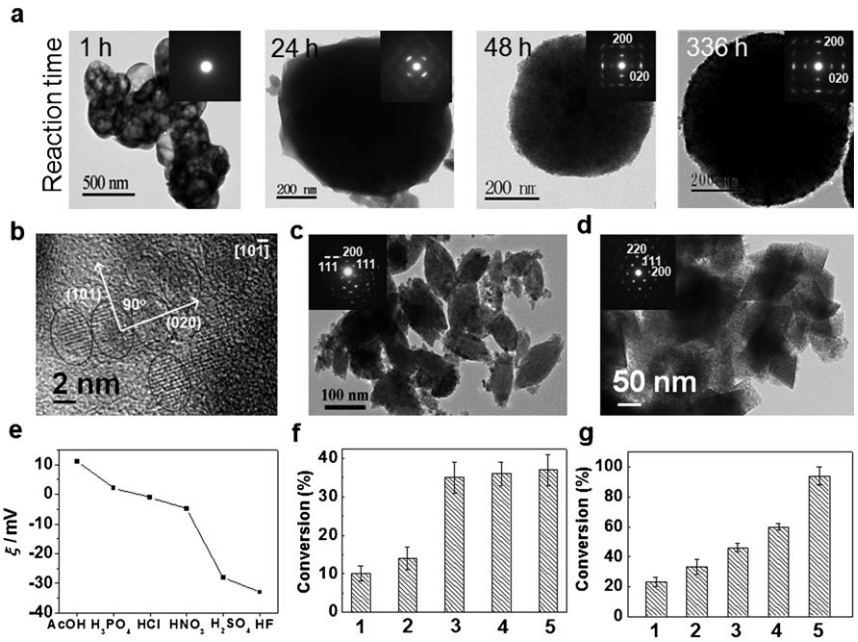

Figure 4. Formation mechanism and photocatalytic activity. a) TEM images of TiO_2 particles synthesized at different reaction times showing a structural evolution from amorphous to crystalline to single crystalline. b) HRTEM image of the TiO_2 building nanocrystals obtained at low precursor concentration. c,d) Representative TEM images and SAED patterns (inset) of mesoporous c) ZrO_2 and d) CeO_2 single crystals, demonstrating the general applicability of this synthesis approach towards a large variety of oxide mesoporous single crystals. The ZrO_2 crystals exhibits a monoclinic structure (space group $P2_1/a$(14), JCPDS No. 37-1484) while the CeO_2 crystals exhibit a cubic structure (space group $Fm3m$(225), JCPDS No. 43-1002). e) ζ potentials of polycrystalline TiO_2 particles dispersed in solution of *tert*-butyl alcohol ($pH \approx 1$) containing AcOH, H_3PO_4, HCl, HNO_3, H_2SO_4, or HF. f) Photocatalytic conversions of the oxidations of toluene to benzaldehyde and g) cinnamyl alcohol to cinnamaldehyde in liquid phase in the presence of 1) commercial P-25, 2) polycrystalline TiO_2, and single-crystal-like TiO_2 with 3) disordered, 4) ordered 2D, and 5) ordered 3D mesoporous structure.

It is important to point out that attached growth has been observed previously,[26,29,30] but never within such mesoscale channels. How do the crystals growing within the individual pore channels communicate and register themselves into a single-crystal configuration? For a KIT-6-like scaffold, the bicontinuous structure naturally enables such communication, although the pore diameter is only 7.8 nm. The SBA-15 scaffold, however, contains cylindrical pores (6.3 nm in diameter) that are arranged in parallel into a 2D hexagonal structure. The communication is believed to be through the pore wall of the scaffold that contains micropores (pore diameter around 1 nm).[31] The growth within these micropores also produces bridges fixing the TiO_2 rods after the scaffold removal.

These unique single-crystal-like TiO_2 mesocages exhibit superior photocatalytic activity and excellent thermal stability (Figure S8). Using the oxidation of toluene to benzaldehyde in liquid phase as an example, we compared the photocatalytic activity of 1) commercial TiO_2 (P-25), 2) polycrystalline TiO_2, and single-crystal-like TiO_2 with 3) disordered, 4) 2D ordered, and 5) 3D ordered mesoporous channels (Figure 4f). The single crystals have comparable surface areas (160–180 $m^2 g^{-1}$) and pore diameter

(3.4–4.5 nm), whereas the polycrystalline sample shows a higher surface area of 200 $m^2 g^{-1}$ and a slightly smaller pore diameter of 2.6 nm (Table S1). As shown, the single-crystal-like TiO_2 samples exhibit two- to threefold increases of activity relative to that of polycrystalline TiO_2 or P-25. To further probe the effect of the crystallographic and porous structure, a larger-size substrate, cinnamyl alcohol, was used. It was found that the conversion of cinnamyl alcohol into cinnamaldehyde systematically increases from photocatalyst 1 to 5 (Figure 4g). Conversion of only 20–30% was achieved for 1 and 2, but almost 100% conversion was achieved for 5, thus confirming that the 3D cage structure endows the catalyst with outstanding performance.

In summary, we synthesized single-crystal-like TiO_2 mesocages with controlled mesoporous structure, preferential active-surface exposure, and superior photocatalytic activity. This synthesis can be readily extended to the synthesis of other oxide single crystals. This work provides a family of functional mesocages for catalysis, energy conversion and storage, and other applications, similar to zeolites, a class of silica-based single crystals with microporous networks.

Experimental Section

Polycrystalline TiO_2 was prepared from a precursor solution of $TiCl_4$ and *tert*-butyl alcohol (molar ratio = 1:165). TiO_2 with disordered mesopores was prepared from a precursor containing $TiOSO_4$ (15 wt% solution in dilute sulfuric acid, purchased from Sigma–Aldrich) and *tert*-butyl alcohol (molar ratio = 1:165). To synthesize TiO_2 with ordered mesopores, $TiOSO_4$ was soaked within the SBA-15 or KIT-6 synthesized using the published procedure[26,27] followed by the addition of *tert*-butyl alcohol (molar ratio of $TiOSO_4$:SiO_2:*tert*-butyl alcohol = 1:20:165). The above precursors were placed in autoclave at 110°C for 48 h. The products were filtered, washed with ethanol, and dried at 100°C. Removal of the SBA-15 and KIT-6 was achieved using 2.0 M NaOH at 80°C followed by centrifugation, washing, and drying. To exclude the sulfate effect on the catalytic studies, sulfate species were completely removed by washing prior to the alkali treatment, as confirmed by elemental analysis (see Table S3 in the Supporting Information).

Received: August 10, 2010
Published online: December 27, 2010

Keywords: adsorption · crystal growth · mesoporous materials · photochemistry · titanium

[1] U. Bach, *Nature* **1998**, *395*, 583–585.
[2] N. Erdman, K. R. Poeppelmeier, M. Asta, O. Warschkow, D. E. Ellis, L. D. Marks, *Nature* **2002**, *419*, 55–58.
[3] M. Grätzel, *Nature* **2001**, *414*, 338–344.
[4] M. Wagemaker, A. P. M. Kentgens, F. M. Mulder, *Nature* **2002**, *418*, 397–399.
[5] H. G. Yang, C. H. Sun, S. Z. Qiao, J. Zou, G. Liu, S. C. Smith, H. M. Cheng, G. Q. Lu, *Nature* **2008**, *453*, 638–641.
[6] P. D. Yang, D. Y. Zhao, D. I. Margolese, B. F. Chmelka, G. D. Stucky, *Nature* **1998**, *396*, 152–155.
[7] Y. Bai, Y. Cao, J. Zhang, M. Wang, R. Li, P. Wang, S. M. Zakeeruddin, M. Grätzel, *Nat. Mater.* **2008**, *7*, 626–630.
[8] D. L. Li, H. S. Zhou, I. Honma, *Nat. Mater.* **2004**, *3*, 65–72.
[9] A. Selloni, *Nat. Mater.* **2008**, *7*, 613–615.
[10] H. Tada, T. Mitsui, T. Kiyonaga, T. Akita, K. Tanaka, *Nat. Mater.* **2006**, *5*, 782–786.
[11] H. Li, Z. Bian, J. Zhu, D. Zhang, G. Li, Y. Huo, H. Li, Y. Lu, *J. Am. Chem. Soc.* **2007**, *129*, 8406–8407.
[12] X. Chen, S. S. Mao, *Chem. Rev.* **2007**, *107*, 2891–2959.
[13] G. Liu, H. G. Yang, X. Wang, L. Cheng, J. Pan, G. Q. Lu, H. M. Cheng, *J. Am. Chem. Soc.* **2009**, *131*, 12868–12869.
[14] Y. Q. Dai, C. M. Cobley, J. Zeng, Y. M. Sun, Y. N. Xia, *Nano Lett.* **2009**, *9*, 2455–2459.
[15] X. Feng, K. Shankar, O. K. Varghese, M. Paulose, T. J. Latempa, C. A. Grimes, *Nano Lett.* **2008**, *8*, 3781–3786.
[16] X. G. Han, Q. Kuang, M. S. Jin, Z. X. Xie, L. S. Zheng, *J. Am. Chem. Soc.* **2009**, *131*, 3152–3153.
[17] B. H. Wu, C. Y. Guo, N. F. Zheng, Z. X. Xie, G. D. Stucky, *J. Am. Chem. Soc.* **2008**, *130*, 17563–17567.
[18] H. G. Yang, G. Liu, S. Z. Qiao, C. H. Sun, Y. G. Jin, S. C. Smith, J. Zou, H. M. Cheng, G. Q. Lu, *J. Am. Chem. Soc.* **2009**, *131*, 4078–4083.
[19] X. Q. Gong, A. Selloni, *J. Phys. Chem. B* **2005**, *109*, 19560–19562.
[20] B. Wang, A. P. Cote, H. Furukawa, M. O'Keeffe, O. M. Yaghi, *Nature* **2008**, *453*, 207–211.
[21] A. Zürner, J. Kirstein, M. Doblinger, C. Brauchle, T. Bein, *Nature* **2007**, *450*, 705–708.
[22] H. K. Chae, D. Y. Siberio-Pérez, J. Kim, Y. B. Go, M. Eddaoudi, A. J. Matzger, M. O'Keeffe, O. M. Yaghi, *Nature* **2004**, *427*, 523–527.
[23] D. Grosso, C. Boissière, B. Smarsly, T. Brezesinski, N. Pinna, P. A. Albouy, H. Amenitsch, M. Antonietti, C. Sanchez, *Nat. Mater.* **2004**, *3*, 787–792.
[24] B. Tian, X. Liu, B. Tu, C. Yu, J. Fan, L. Wang, S. Xie, G. D. Stucky, D. Zhao, *Nat. Mater.* **2003**, *2*, 159–163.
[25] J. C. Yu, X. C. Wang, X. Z. Fu, *Chem. Mater.* **2004**, *16*, 1523–1530.
[26] Z. R. Tian, J. Liu, J. A. Voigt, B. Mckenzie1, H. Xu, *Angew. Chem.* **2003**, *115*, 429–433; *Angew. Chem. Int. Ed.* **2003**, *42*, 413–417.
[27] D. Zhao, J. Feng, Q. Huo, N. Melosh, G. H. Fredrickson, B. F. Chmelka, G. D. Stucky, *Science* **1998**, *279*, 548–552.
[28] F. Kleitz, S. H. Choi, R. Ryoo, *Chem.Commun.* **2003**, 2136–2137.
[29] M. Niederberger, H. Colfen, *Phys. Chem. Chem. Phys.* **2006**, *8*, 3271–3287.
[30] M. Adachi, Y. Murata, J. Takao, J. Jiu, M. Sakamoto, F. Wang, *J. Am. Chem. Soc.* **2004**, *126*, 14943–14949.
[31] S. H. Joo, S. J. Choi, I. Oh, J. Kwak, Z. Liu, O. Terasaki, R. Ryoo, *Nature* **2001**, *412*, 169–172.

